Nanoscale

COMMUNICATION

View Article Online
View Journal | View Issue

Cite this: *Nanoscale*, 2016, **8**, 12693

Received 14th April 2016,
Accepted 27th May 2016

DOI: 10.1039/c6nr03096c

www.rsc.org/nanoscale

Gold nanoparticle capture within protein crystal scaffolds†

Ann E. Kowalski,[a] Thaddaus R. Huber,[a] Thomas W. Ni,[b] Luke F. Hartje,[c] Karina L. Appel,[a] Jarad W. Yost,[a] Christopher J. Ackerson[b] and Christopher D. Snow*[a]

DNA assemblies have been used to organize inorganic nanoparticles into 3D arrays, with emergent properties arising as a result of nanoparticle spacing and geometry. We report here the use of engineered protein crystals as an alternative approach to biologically mediated assembly of inorganic nanoparticles. The protein crystal's 13 nm diameter pores result in an 80% solvent content and display hexahistidine sequences on their interior. The hexahistidine sequence captures Au_{25}(glutathione)$_{\sim 17}$ (nitrilotriacetic acid)$_{\sim 1}$ nanoclusters throughout a chemically crosslinked crystal *via* the coordination of Ni(II) to both the cluster and the protein. Nanoparticle loading was validated by confocal microscopy and elemental analysis. The nanoparticles may be released from the crystal by exposure to EDTA, which chelates the Ni(II) and breaks the specific protein/nanoparticle interaction. The integrity of the protein crystals after crosslinking and nanoparticle capture was confirmed by single crystal X-ray crystallography.

The optical and magnetic properties of inorganic nanoparticles, which are already quite different than their corresponding bulk-phase counterparts, are further modified in ordered assemblies.[1,2] These changes depend on the distance between particles, and in the case of anisotropic particles, the orientation of particles relative to each other.[3,4] The application of nanoparticle assemblies is realized in biomedicine, for instance in diagnostics.[5]

The use of biological scaffolds to enforce particle assembly is well established in the case of DNA oligonucleotides.[6] Both DNA origami[7–9] and cDNA based approaches[6,10] have been used to control the assembly of gold nanoclusters. The use of proteins to organize nanoparticles is less well established, in part because protein oligomer assembly structures are harder to predict than DNA nanostructure. Still, notable examples of protein organization of nanoparticles include the use of viruses to organize particles,[11–13] and the use of multimeric proteins.[14–18] Also, Kostiainen *et al.* prepared binary superlattices by co-assembling protein cages with nanoparticles.[19]

In contrast, we focus here on organizing metallic nanoparticles in three dimensions within pre-existing crosslinked crystals. Compared to other scaffold materials, crosslinked protein crystals offer potential advantages in terms of stability and precision in the face of changing solvent conditions. Nonetheless, protein crystals represent a less explored scaffold for organizing metallic nanoparticles in three dimensions.[20,21] A key challenge, uptake of the guest particles into the crystal, depends on the size of the particles with respect to the solvent channels of the crystal. These pores are often used to facilitate diffusion of cofactors, drugs, and substrates into crystals, in order to observe the biological effects of these molecules in single crystal X-ray structural studies.[22] Diffusion of metals into crystals is also used in metal based phasing methods such as multiple anomalous dispersion and multiple isomorphous replacement.[23–25] Indeed, small metal clusters were used for phasing the largest biomacromolecules solved by single-crystal X-ray methods.[26]

To our knowledge, this report is the first example of controlled adsorption of larger nanoparticles into a pre-existing protein crystal. The conventional 'soaking' of metal coordination complexes and clusters into crystals for phasing relies on serendipitous binding; the metals do not adsorb to specified sites.[27] In contrast, we present the first example of capture of nanoparticles inside a pre-existing protein crystal *via* a specific metal-mediated interaction. A key benefit of metal-based capture motifs is the relative ease of generalizing the capture motif to other guest molecules.

To accomplish the uptake of nanoparticles (specifically $Au_{25}(GSH)_{17}$(NTA) clusters), we used a host crystal with large pores (Fig. 1a). Control experiments (below) suggest that the guest particles are tethered to the host crystal *via* surface NTA groups that bind Ni(II) atoms that are also coordinated by hexahistidine metal affinity tags (histag) presented at specific locations within the host crystal (Fig. 1b).[28,29] The interaction

[a]*Department of Chemical and Biological Engineering, Colorado State University, Fort Collins, CO 80521, USA. E-mail: Christopher.Snow@Colostate.edu*
[b]*Department of Chemistry, Colorado State University, Fort Collins, CO 80521, USA*
[c]*Department of Biochemistry and Molecular Biology, Colorado State University, Fort Collins, CO 80523, USA*

†Electronic supplementary information (ESI) available: Complete experimental details and supplementary figures and tables. See DOI: 10.1039/c6nr03096c

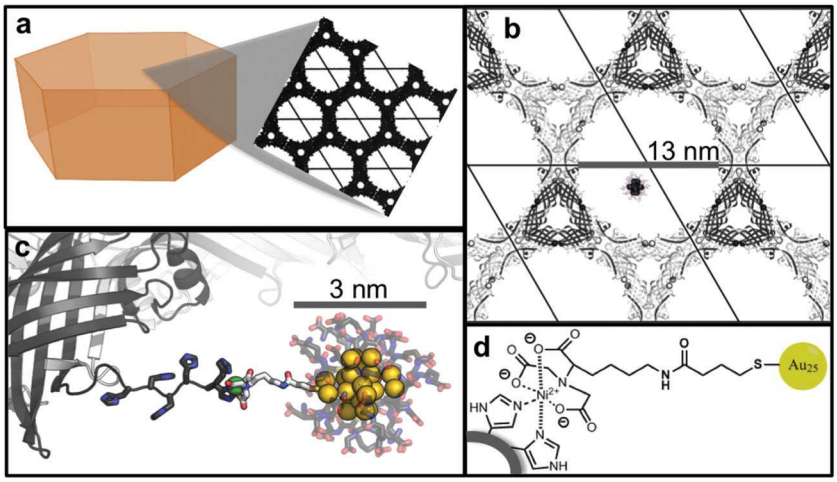

Fig. 1 (a) CJ crystals offer a hexagonal array of large axial pores. (b) The 13 nm diameter of these pores is much larger than the guest nanoparticles. (c) & (d) The host crystal can capture the guest nanoparticles *via* shared metal affinity.

is specific and reversible. With the availability of increasingly powerful algorithms for protein design,[30–32] porous protein crystal scaffolding may approach, or even surpass, the ability of DNA to spatially localize inorganic nanoparticles.

The host protein crystal was selected in a systematic, automated screen of the Protein Data Bank for protein crystals with large solvent channels (Fig. 1a). The crystal selected from the database is composed of a single protein, CJ0 (Genebank ID: cj0420, Protein Data Bank (PDB) code: 2fgs). CJ0 is a putative periplasmic polyisoprenoid-binding protein from *Campylobacter jejuni*. The vector encoding CJ0 (Fig. S1†) was obtained from Protein Structure Initiative: Biology-Materials Repository. For ease of uniform expression and purification, the periplasmic signaling peptide was deleted, yielding the target gene, CJ. CJ has a C-terminal histag and is encoded in expression vector pSB3.[33] CJ crystals were grown in mTacsimate™ buffer (Fig. S3†) at pH 7.5 and crosslinked by direct addition of 1% glyoxal and 25 mM dimethyl amine borane complex (DMAB). The crosslinking reaction was quenched after two hours *via* addition of 0.3 M hydroxylamine and 25 mM DMAB at pH 5.0.

Crosslinked CJ crystals readily absorbed $Au_{25}(GSH)_{17}$(NTA) and $Au_{25}(GSH)_{18}$, as judged by intrinsic nanoparticle fluorescence (Fig. 2 and 3).[34] Fig. 2 shows typical crystals at the end of a 30 minute incubation in each gold nanoparticle solution. The time it takes for the solution to completely penetrate the crystal varies with solution concentration and crystal thickness. However, the nanoparticles generally "load" into the crystals within about 30 minutes, as judged by confocal cross-section (Fig. 3). Fig. 2 demonstrates that the nanoparticle NTA, the scaffold histag, and Ni(II) all must be present to retain the nanoparticle within the crystal pore. For example, crystals lacking a histag (CJΔH6) lost $Au_{25}(GSH)_{17}$(NTA) within 4 days (Fig. 2a–c), even in the presence of Ni(II). In the absence of Ni(II), release of $Au_{25}(GSH)_{17}$(NTA) from CJ crystals does not require EDTA (Fig. S5†).

Confocal laser microscopy (CLM) and elemental analysis were used to quantify loading of the crystals. A CJ crystal was

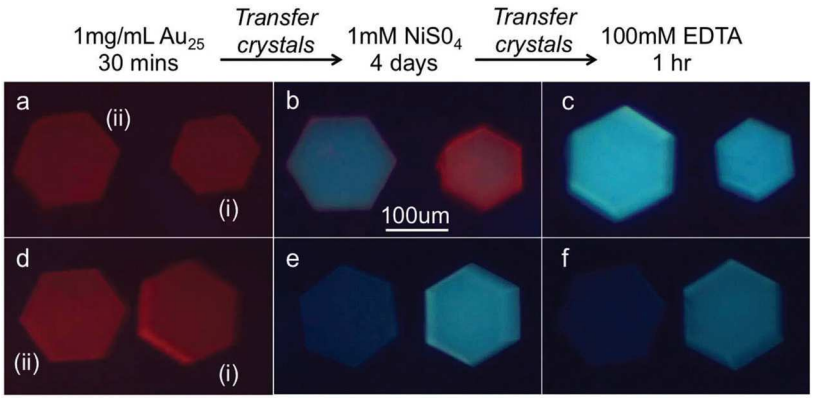

Fig. 2 Each image contains a (i) CJ and (ii) CJΔH6 crystal. (a) At t = 30 in 1 mg ml^{-1} $Au_{25}(GSH)_{17}$(NTA). (b) At t = 4 days in 1 mM $NiSO_4$ at pH 7.0. (c) At t = 1 h in 0.1 M EDTA at pH 7.0. (d) & (e) & (f) Same as (a) & (b) & (c) respectively except with $Au_{25}(GSH)_{18}$. Imaged with a 405 nm laser and a 450 nm longpass filter.[34]

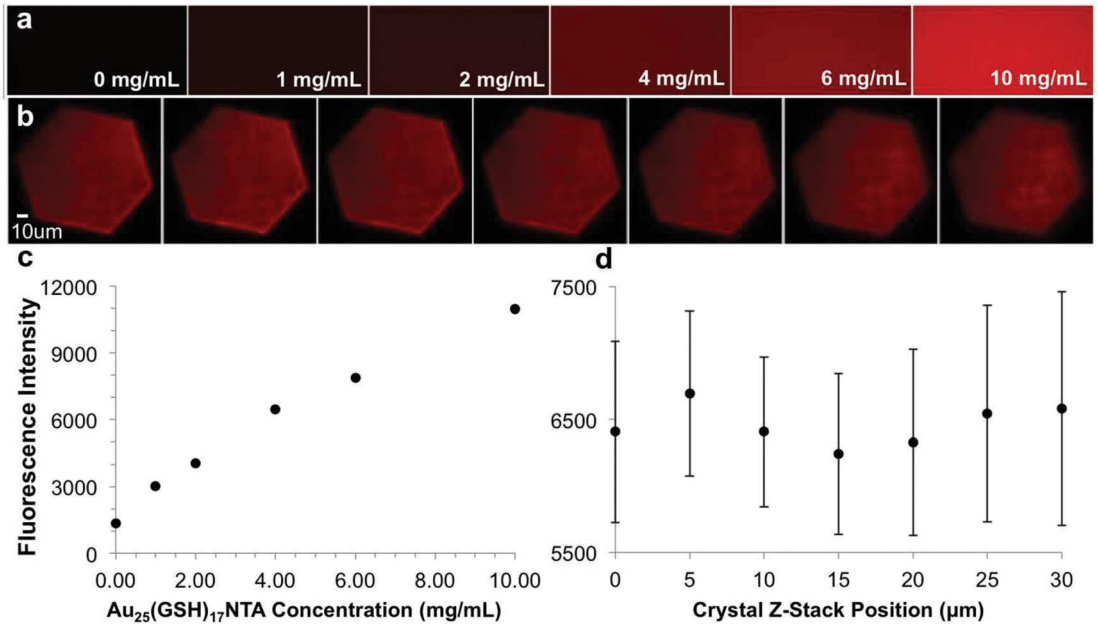

Fig. 3 (a) Confocal laser microscopy (CLM) images of $Au_{25}(GSH)_{17}$(NTA) fluorescence standards: 0, 1, 2, 4, 6, and 10 mg ml^{-1} (left to right). (b) CLM *z*-stack showing $Au_{25}(GSH)_{17}$(NTA) fully loaded into a CJ protein crystal. The crystal was soaked in 1 mg ml^{-1} $Au_{25}(GSH)_{17}$(NTA) for 30 minutes, then incubated in 1 mm $NiSO_4$ for five days prior to imaging. The 30 μm *z*-stack was taken through the crystal from the top surface (left) to the bottom surface (right) at 5 μm intervals. (c) Fluorescence intensity standard curve created by averaging $Au_{25}(GSH)_{17}$(NTA) intensities from (a). (d) Average fluorescence intensity of crystal cross-sections from (b). When compared to the fluorescence intensity standard curve in (c), the crystal is shown to retain an average $Au_{25}(GSH)_{17}$(NTA) concentration of 4.7 ± 0.7 mg ml^{-1}. all images were taken under identical optical settings and excited with a 561 nm diode laser, chosen for lower background fluorescence (see ESI†).

incubated for 30 minutes with $Au_{25}(GSH)_{17}$(NTA), then transferred to a 50 μl reservoir containing 1 mM Ni(II) and incubated for five days. CLM shows retention of gold nanoparticles throughout the entire thickness of the crystal (Fig. 3). A CLM fluorescence intensity standard curve was created and used to interpolate an estimated concentration of $Au_{25}(GSH)_{17}$(NTA) within the crystal. The fluorescence intensity of gold nanoparticle solutions ranging from 0 mg mL^{-1} to 10 mg mL^{-1} was measured. Comparing these values to the fluorescence intensity inside the crystal *z*-stack, we found that after 30 minutes of loading and a five day incubation in $NiSO_4$, gold nanoparticles adsorbed to an average of 4.7 ± 0.7 mg mL^{-1} within the crystal pores. This concentration is roughly equivalent to one $Au_{25}(GSH)_{17}$(NTA) cluster per two unit cells. Elemental analysis confirmed the adsorption of gold nanoparticles per unit cell of the crystal at various timepoints during loading and unloading (Fig. S10†). At the most concentrated timepoints (t = 48 hours), elemental analysis suggested an average of 12 nanoparticles per unit cell in the crystal, a 118.5 mg mL^{-1} concentration *in crystallo*.

Time lapse confocal loading data suggests that strong adsorption is complicating guest diffusion (Fig. S7†). Simple concentration-independent diffusion models with a fixed surface concentration boundary condition predict a guest concentration gradient that decreases with time as the concentration in the crystal center approaches that of the layers closer to the external solution. In stark contrast, we observe a guest nanoparticle concentration gradient that increases over the first hour of loading. To better explain diffusion in the system, we are currently developing concentration-dependent continuum models and multi-scale molecular models. These will be the subject of an upcoming publication.

Crystal quality after crosslinking and $Au_{25}(GSH)_{17}$(NTA) loading and unloading was assessed by single crystal X-ray diffraction (Fig. S8†). Crystal diffraction was retained to ~4.2 Å resolution with 1.2° mosaicity. Retention of crystal integrity after full loading of gold nanoparticles indicated that the CJ protein crystal nanopores remained intact and provided a robust scaffold for reversible, site-specific gold nanoparticle capture. However, $Au_{25}(GSH)_{17}$(NTA) was not visible in the XRD electron density map (Fig. S9†). This result is consistent with the nanoparticles adopting heterogeneous positions within the crystal. In order to resolve the gold nanoparticle structure on the protein crystal scaffold, further efforts are underway. Specifically, we will attempt to replace the histag : NTA interaction motif with capture motifs that have fewer degrees of freedom.

Conclusions

We have immobilized gold nanoparticles using precisely spaced motifs within a robust array of 13 nm nanopores (Fig. S9†) delimited by a highly porous (80% solvent) protein

crystal (ESI Appendix†). Scaffold formation was robust, and crystals could be grown and crosslinked with and without histags. CLM indicated long-term (>5 days), Ni(II) dependent capture throughout the entire thickness of the crystal. Elemental analysis confirmed increasing adsorption of gold nanoparticles within the protein crystal pores over time, as well as removal upon addition of EDTA. Both elemental analysis and fluorescence intensity from CLM show that gold nanoparticles are absorbed into the crystal beyond concentrations expected through pure diffusion (ESI Appendix†). The attachment is specific and reversible, the same crystal scaffold can be repeatedly loaded and unloaded with $Au_{25}(GSH)_{17}(NTA)$, (Fig. S6†) and the crystal retains X-ray diffraction quality throughout loading and unloading of nanoparticles.

Notes and references

1 L. Wang, L. Xu, H. Kuang, C. Xu and N. A. Kotov, *Acc. Chem. Res.*, 2012, **45**, 1916–1926.
2 C. A. Mirkin, R. L. Letsinger, R. C. Mucic and J. J. Storhoff, *Nature*, 1996, **382**, 607–609.
3 A. M. Funston, C. Novo, T. J. Davis and P. Mulvaney, *Nano Lett.*, 2009, **9**, 1651–1658.
4 L. S. Slaughter, *et al.*, *Nano Lett.*, 2012, **12**, 3967–3972.
5 J.-M. Nam, S. I. Stoeva and C. A. Mirkin, *J. Am. Chem. Soc.*, 2004, **126**, 5932–5933.
6 A. P. Alivisatos, *et al.*, *Nature*, 1996, **382**, 609–611.
7 B. Ding, *et al.*, *J. Am. Chem. Soc.*, 2010, **132**, 3248–3249.
8 P. W. K. Rothemund, *Nature*, 2006, **440**, 297–302.
9 W. Liu, *et al.*, *Science*, 2016, **351**, 582–586.
10 C. J. Ackerson, M. T. Sykes and R. D. Kornberg, *Proc. Natl. Acad. Sci. U. S. A.*, 2005, **102**, 13383–13385.
11 P. Y. Chen, *et al.*, *ACS Nano*, 2013, **7**, 6563–6574.
12 Y. Huang, *et al.*, *Nano Lett.*, 2005, **5**, 1429–1434.
13 A. Szuchmacher, *et al.*, *Nano Lett.*, 2004, **4**, 867–870.
14 C. J. Ackerson, P. D. Jadzinsky, G. J. Jensen and R. D. Kornberg, *J. Am. Chem. Soc.*, 2006, **128**, 2635–2640.
15 J. Z. Sexton and C. J. Ackerson, *J. Phys. Chem. C*, 2010, **114**, 16037–16042.
16 F. Baneyx and J. F. Matthaei, *Curr. Opin. Biotechnol.*, 2014, **28**, 39–45.
17 M. Sarikaya, C. Tamerler, A. K.-Y. Jen, K. Schulten and F. Baneyx, *Nat. Mater.*, 2003, **2**, 577–585.
18 H. Gradišar, *et al.*, *Nat. Chem. Biol.*, 2013, **9**, 362–366.
19 M. Kostiainen, *et al.*, *Nat. Nanotechnol.*, 2013, **8**, 52–56.
20 S. Abe, *et al.*, *Small Weinh. Bergstr. Ger.*, 2012, **8**, 1314–1319.
21 T. Koshiyama, *et al.*, *Bioconjugate Chem.*, 2010, **21**, 264–269.
22 I. R. Krauss, A. Merlino, A. Vergara and F. Sica, *Int. J. Mol. Sci.*, 2013, **14**, 11643–11691.
23 A. Szöke, H. Szöke and J. R. Somoza, *Acta Crystallogr., Sect. A: Fundam. Crystallogr.*, 1997, **53**, 291–313.
24 J. Karle, *Int. J. Quantum Chem.*, 1980, **18**, 357–367.
25 G. Kartha and R. Parthasarathy, *Acta Crystallogr.*, 1965, **18**, 745–749.
26 A. L. Gnatt, P. Cramer, J. Fu, D. A. Bushnell and R. D. Kornberg, *Science*, 2001, **292**, 1876–1882.
27 Y. Takeda, T. Kondow and F. Mafuné, *Chem. Phys. Lett.*, 2011, **504**, 175–179.
28 S. Uchinomiya, *et al.*, *Chem. Commun.*, 2009, 5880–5882.
29 J. F. Hainfeld, W. Liu, C. M. Halsey, P. Freimuth and R. D. Powell, *J. Struct. Biol.*, 1999, **127**, 185–198.
30 S. Park, X. Yang and J. G. Saven, *Curr. Opin. Struct. Biol.*, 2004, **14**, 487–494.
31 J. G. Saven, *Curr. Opin. Colloid Interface Sci.*, 2010, **15**, 13–17.
32 N. Pokala and T. M. Handel, *J. Struct. Biol.*, 2001, **134**, 269–281.
33 DNASU Plasmid | Detailed Vector Information: pSB3. *DNASU Plasmids* at <http://dnasu.org/DNASU/GetVectorDetail.do?vectorid=383>.
34 Z. Wu and R. Jin, *Nano Lett.*, 2010, **10**, 2568–2573.

